PNAS RESEARCH ARTICLE | MEDICAL SCIENCES

Antibody-mediated blockade for galectin-3 binding protein in tumor secretome abrogates PDAC metastasis

Yeon-Sook Choi[a,1], Myung Ji Kim[a,1], Eun A. Choi[a], Sinae Kim[a], Eun ji Lee[a], Min Ji Park[a], Mi-Ju Kim[b], Yeon Wook Kim[b], Hee-Sung Ahn[c], Jae Yun Jung[a], Gayoung Jang[a], Yongsub Kim[a], Hyori Kim[c], Kyunggon Kim[c], Jin Young Kim[d], Seung-Mo Hong[e], Song Cheol Kim[f,2], and Suhwan Chang[a,2]

Edited by Mariano Barbacid, Centro Nacional de Investigaciones Oncologicas, Madrid, Spain; received October 18, 2021; accepted April 27, 2022

The major challenges in pancreatic ductal adenocarcinoma (PDAC) management are local or distant metastasis and limited targeted therapeutics to prevent it. To identify a druggable target in tumor secretome and to explore its therapeutic intervention, we performed a liquid chromatography–tandem mass spectrometry (LC-MS/MS)–based proteomic analysis of tumors obtained from a patient-derived xenograft model of PDAC. Galectin-3 binding protein (Gal-3BP) is identified as a highly secreted protein, and its overexpression is further validated in multiple PDAC tumors and primary cells. Knockdown and exogenous treatment of Gal-3BP showed that it is required for PDAC cell proliferation, migration, and invasion. Mechanistically, we revealed that Gal-3BP enhances galectin-3–mediated epidermal growth factor receptor signaling, leading to increased cMyc and epithelial-mesenchymal transition. To explore the clinical impact of these findings, two antibody clones were developed, and they profoundly abrogated the metastasis of PDAC cells in vivo. Altogether, our data demonstrate that Gal-3BP is an important therapeutic target in PDAC, and we propose its blockade by antibody as a therapeutic option for suppressing PDAC metastasis.

pancreatic cancer | metastasis | galectin-3 binding protein | blocking antibody | tumor secretome

Significance

Pancreatic ductal adenocarcinoma (PDAC) metastasis is a major cause for poor prognosis; therefore, developing targeted therapeutics is critical for overcoming it. By proteomic analysis of tumor secretome, we identified the galectin-3 binding protein as a druggable target for PDAC metastasis. Further, we developed an antibody for the galectin-3 binding protein and showed that the antibody-mediated blockade is a promising therapeutic strategy for PDAC.

One of the challenges faced in pancreatic ductal adenocarcinoma (PDAC) management is the absence of targeted therapeutics (1, 2). Thus, finding a druggable target is critical. In addition to the mutant K-Ras, which has been identified as a dominant driver and therapeutic target in recent studies (3, 4), multiple targets including epidermal growth factor receptor (EGFR), PI3K, Raf, MEK(Mitogen Activated Protein Kinase-Kinase), and tumor growth factor beta are being investigated (5, 6). However, the clinical application of these target proteins is still under investigation, and the strategies used for targeting the proteins do not take into consideration the genetic and intratumoral heterogeneity of PDAC (1, 7).

The tumor secretome (8, 9) is an important source of therapeutic or diagnostic targets. As tumor-derived proteins or bioactive molecules are often diluted in the blood, the detection of a locally secreted protein is an attractive alternative method for identifying novel target proteins (10). In practice, analyses of the interstitial fluid obtained from tumor (11) have revealed the enrichment of cytokines in breast cancer (12), S100A in cholangiocarcinoma (13), and Fascin in head and neck cancer (14). Considering the presence of a stromal-rich microenvironment (15) and intricate communication between PDAC and stellate cells (2, 16), an investigation of tumor interstitial fluid (TIF) and antifibrotic therapy in pancreatic cancer seems promising (17). Indeed, a recent study demonstrated that the metabolite profile of PDAC-TIF is distinct from that of the plasma (18). Despite the potential advantages associated with analyzing the TIF, few reports exist regarding the proteomic analysis of PDAC-TIF. This might be due to the difficulty in obtaining fresh PDAC tissue for TIF isolation. Moreover, the high variability in the proteomic profiles of individual tumors makes it necessary to investigate large numbers of specimens for achieving a statistical significance. To circumvent these limitations, we developed a patient-derived xenograft (PDX) model of PDAC (19) and compared the TIF proteome data with those of breast cancer PDX (20), thereby ensuring PDAC-specific or PDAC-enriched target identification.

Galectin-3 binding protein (Gal-3BP) is a highly glycosylated protein that has been identified in multiple screening studies investigating tumor-secretory proteins in melanoma (21), lung carcinoma (22), and breast cancer (23). Apart from galectin-3, Gal-3BP can also interact with galectin-1; β1-integrins; and extracellular matrix proteins, including collagen, fibronectin, and laminin (24). In cancer, Gal-3BP is mainly involved in cell–matrix or cell–cell interactions and affects metastasis or tumor cell–stromal cell communication (25, 26). Despite extensive research, the role of Gal-3BP in pancreatic cancer remains largely unknown, probably because Gal3-BP is expressed at low levels in the pancreas under normal conditions (from public data; available at https://www.

Author affiliations: [a]Department of Biomedical Sciences, University of Ulsan College of Medicine, Asan Medical Center, Seoul 05505, South Korea; [b]Asan Institute for Life Sciences, Asan Medical Center, Seoul, 05505, South Korea; [c]Department of Convergence Medicine, University of Ulsan College of Medicine, Asan Medical Center, Seoul 05505, South Korea; [d]Research Center for Bioconvergence Analysis, Korea Basic Science Institute, Ochang, 28119, South Korea; [e]Department of Pathology, University of Ulsan College of Medicine, Asan Medical Center, Seoul 05505, South Korea; and [f]Division of Hepato-Biliary and Pancreatic Surgery, Department of Surgery, University of Ulsan College of Medicine, Asan Medical Center, Seoul 05505, South Korea

Author contributions: S.C.K. and S.C. designed research; Y.-S.C., M.J.K., E.A.C., S.K., M.-J.K., and H.-S.A. performed research; Y.-S.C., M.J.K., E.j.L., M.J.P., Y.W.K., J.Y.J., G.J., Y.K., H.K., K.K., and S.-M.H. contributed new reagents/analytic tools; Y.-S.C., S.K., M.J.K., H.-S.A., H.K., K.K., J.Y.K., S.-M.H., and S.C. analyzed data; and S.C.K. and S.C. wrote the paper.

The authors declare no competing interest.

This article is a PNAS Direct Submission.

[1]Y.-S.C. and M.J.K. contributed equally to this work.

[2]To whom correspondence may be addressed. Email: suhwan.chang@amc.seoul.kr or drksc@amc.seoul.kr.

This article contains supporting information online at http://www.pnas.org/lookup/suppl/doi:10.1073/pnas.2119048119/-/DCSupplemental.

Published July 18, 2022.

proteinatlas.org/ENSG00000108679-LGALS3BP/tissue). In this study, we identified high levels of Gal-3BP in PDAC-TIF. Furthermore, the results of this study reveal a function of Gal-3BP in PDAC and indicate that antibody-mediated Gal-3BP blockade might serve as a promising therapeutic strategy against PDAC.

Results

Identification of Gal-3BP as a Secreted Protein in the TIF via Proteomic Analysis of the PDAC PDX Model. To identify a cancer-specific druggable protein target in the pancreas, we analyzed three TIFs obtained from the PDX model of PDAC, along with three TIFs from breast cancer PDX models. In the initial analysis using liquid chromatography–tandem mass spectrometry (LC-MS/MS), 1,413 proteins for PDAC and 1,822 proteins for breast PDX were detected (Fig. 1*A*). Among them, 87 proteins were expressed at higher levels in PDAC (cutoff 2.5-fold; *SI Appendix*, Table S1 for raw data) compared to those in the breast. Based on the upregulated fold and literature search for subcellular localization, we selected two secreted proteins: LGALS3BP and progranulin (PGRN). The increased expression of Gal-3BP and PGRN in PDAC TIFs was confirmed (Fig. 1*B*). Moreover, high levels of these proteins were observed in the culture media of PDAC cells but not in normal HPDE(Human Pancreatic Ductal Epithelial) cells, suggesting tumor-specific, active secretion (Fig. 1*C*). Consistent with their enhanced secretion, the two candidate targets showed elevated expression at the protein (Fig. 1*D*) and messenger RNA (mRNA) levels (Fig. 1*E*). Further, Gal-3BP—but not PGRN—was detected in the plasma of the PDX model (Fig. 1*F*); this suggested that Gal-3BP can be detected in liquid biopsy samples. Therefore, we focused on Gal-3BP for further study. The upregulated Gal-3BP in PDAC was validated in 10 pairs of frozen normal/tumor specimens (*SI Appendix*, Fig. S1*A*). Moreover, plasma analysis of 25 PDAC patients by MRM (multiple reaction monitoring; ref. 27) revealed Gal-3BPs are upregulated compared to the plasma of breast patients (*SI Appendix*, Fig. S1*B* and *C*; $n = 32$; *SI Appendix*, Table S2 for raw data). Lastly, immunohistochemical (IHC) analysis of tissue microarray (TMA) containing PDAC ($n = 153$) and matched normal ($n = 21$) validated our finding (Fig. 1*G* and *SI Appendix*, Fig. S2 for raw data), indicating the Gal-3BP is significantly overexpressed in PDAC compared to normal tissue (Fig. 1*H* for averaged score; see *SI Appendix*, Table S3 for the scores of each tumor).

Stable Knockdown of Gal-3BP Significantly Reduces the Growth and Tumorigenic Potential of PDAC Cells. Upregulation of galectin-1 and galectin-3 has been observed in cancer (28, 29). Considering the primary binding partners of Gal-3BP are

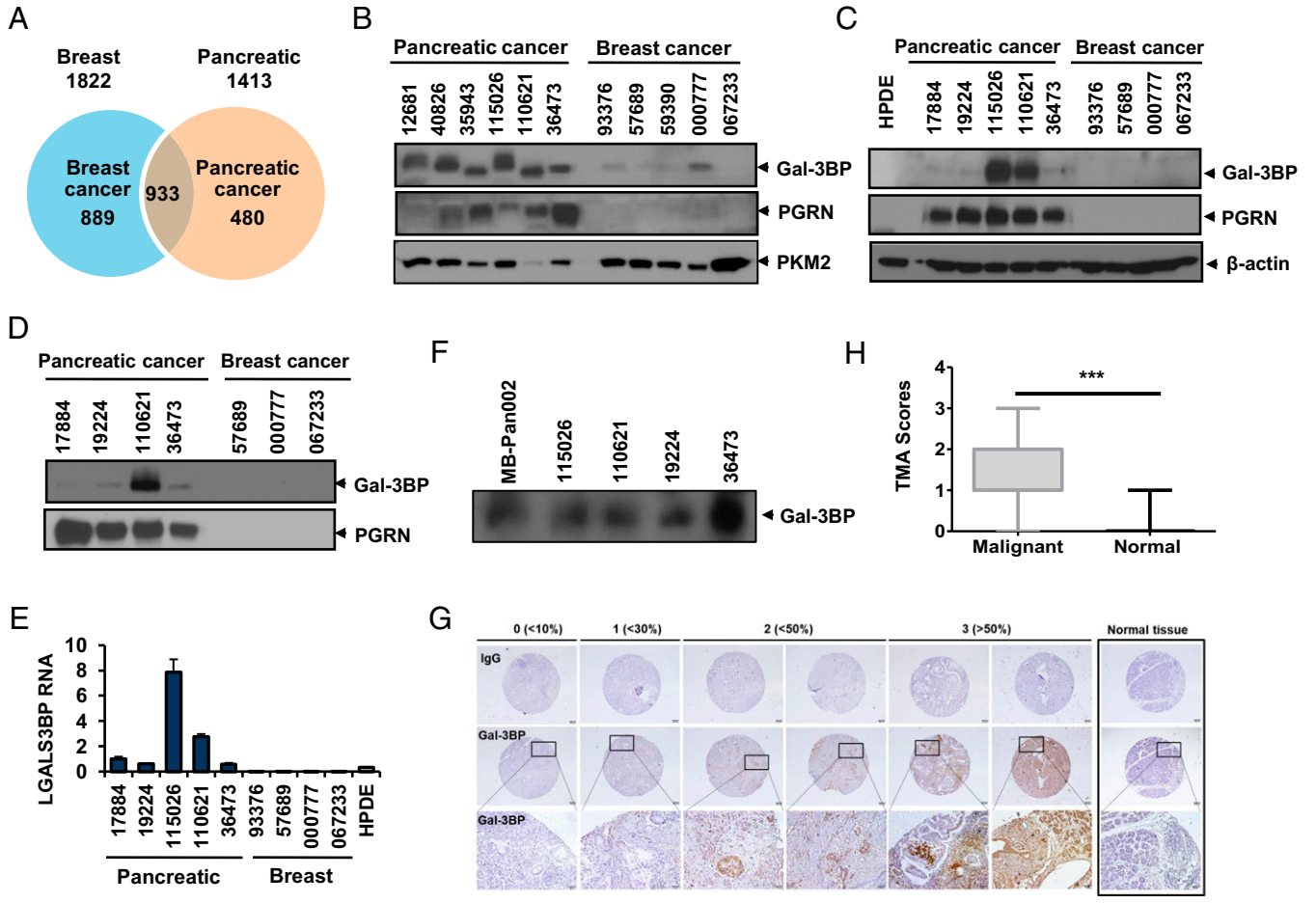

Fig. 1. Identification of Gal-3BP, highly secreted in PDAC, by proteomic analysis. (*A*) Venn diagram depicting the number of proteins quantified via LC-MS/MS analyses. (*B* and *C*) Western blot–mediated validation of Gal-3BP and PGRN identified from TIFs (*B*) and conditioned media from cancer primary cells (*C*). (*D* and *E*) Secreted Gal-3BP (*D*) or intracellular mRNA (*E*) level from five pancreatic cancer cell primary cells, four breast cancer primary cells, and normal pancreatic ductal epithelial cells (HPDE). (*F*) Detection of Gal-3BP from PDX plasma samples depleted with albumin and IgG. (*G*) Representative staining images and grading of TMA comprising PDAC ($n = 153$) and matched normal ($n = 21$). Bottom panels present enlarged part of insets marked in the middle panels. Scale bar: 200 μm (*Top* and *Middle*) and 50 μm (*Bottom*). (*H*) A graph showing averaged grade of Gal-3BP staining obtained from the TMA images ($n = 7$ per group). See *SI Appendix*, Fig. S2 for raw data.

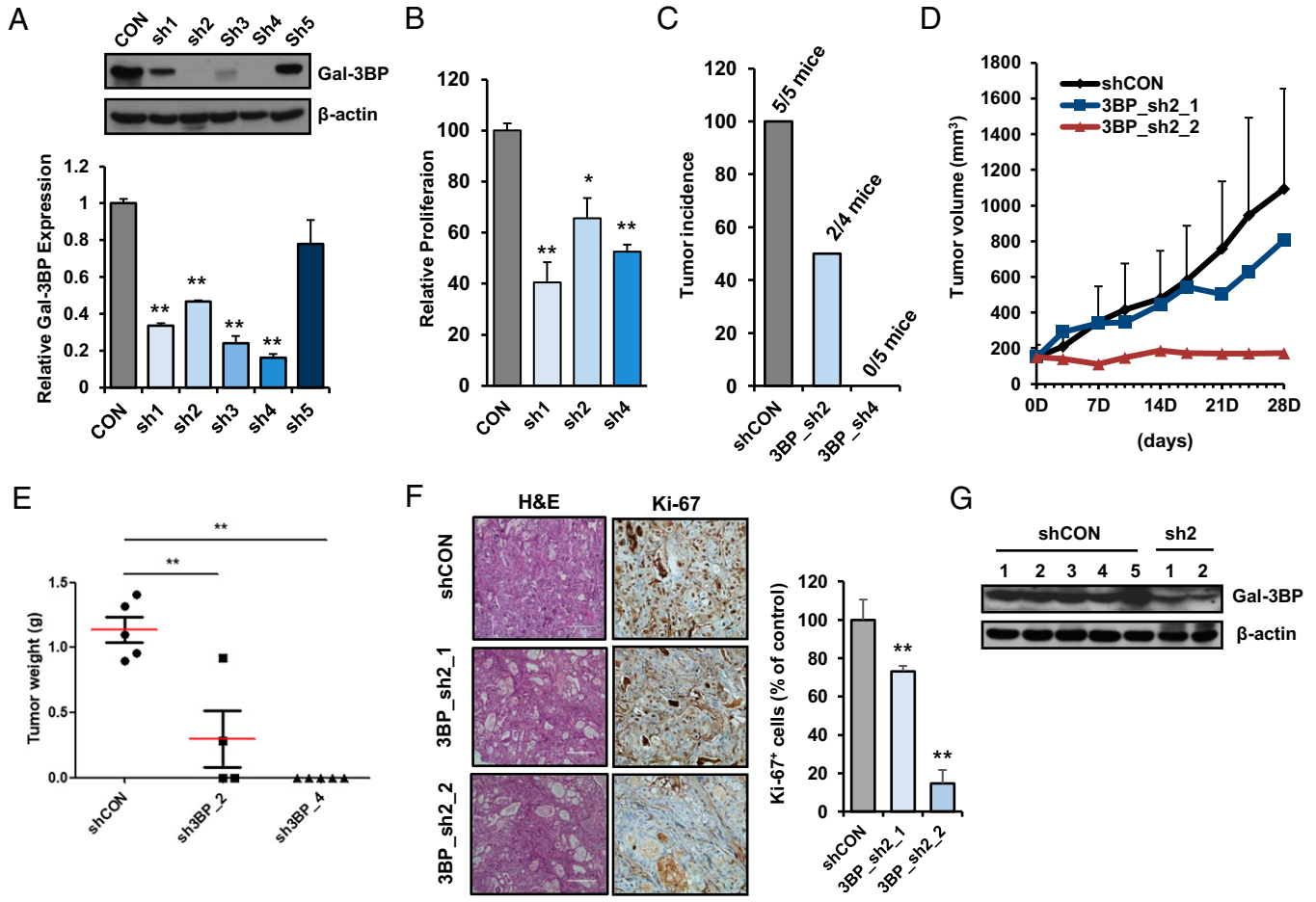

Fig. 2. Knockdown of Gal-3BP in PDAC cells attenuates proliferation and tumor formation. (*A*) Tumor formation upon the subcutaneous injection of 110621 cells transfected with control shRNA or LGALS3BP shRNA. (*B*) Growth curves of 110621 tumors following subcutaneous injection of tumor cells. Black line indicates the average tumor size in mice injected with shRNA control-transfected cells ($n = 5$). The red and blue lines represent the tumor size in each of the two 3BP_sh2 groups. (*C*) Tumor formation upon subcutaneous injection of 110621 cells transfected with control shRNA or LGALS3BP shRNA. (*D*) Growth curves of 110621 tumors following subcutaneous injection of tumor cells. Black line indicates average tumor size in mice injected with shRNA control-transfected cells ($n = 5$). The red and blue lines represent the tumor size in each of the two 3BP_sh2 groups. (*E*) Ex vivo measurement of tumor weight. (*F*) IHC depicting Ki67 expression in subcutaneous tumor tissues. Scale bar: 100 μm. Quantified data were determined based on the number of K_i-67–positive cells. (*G*) Protein expression analysis of LGALS3BP in tissue lysates from subcutaneous tumor tissue. See *SI Appendix*, Fig. S3 for additional PDC data.

galectin-1 and galectin-3, we first investigated the function of Gal-3BP with respect to cell proliferation by knocking it down in primary PDAC cells. Fig. 2*A* depicts the expression of Gal-3BP at the mRNA (graph) and protein levels (upper panel) after stable knockdown. In three independent stable cell lines expressing short hairpin RNA (shRNA) against Gal-3BP, significantly attenuated cancer cell proliferation was observed (Fig. 2*B*). Importantly, when two of the stable cell lines were transplanted into nude mice, the tumor formation rate was dramatically reduced (Fig. 2*C*), compared to that in mice transplanted with wild-type cells (2 tumors versus 10). Moreover, the two tumors formed upon injecting the 3BP_Sh2 cell line showed slower growth (Fig. 2*D*) and low weight (Fig. 2*E*). Further analysis confirmed the reduced expression of Gal-3BP (Fig. 2*G*) and K_i-67 in the tumor (Fig. 2*F*). The reduced tumorigenic potential by Galk-3BP depletion was further confirmed in another primary PDAC cell, 110526 (*SI Appendix*, Fig. S3). These data suggest that Gal-3BP is required for PDAC cell growth both in vitro and in vivo.

Gal-3BP Knockdown Significantly Reduces the Adhesion and Migration of PDAC Cells. A previous study reported that the silencing of galectin-3 results in suppressed pancreatic cancer cell migration (30). However, the effect of Gal-3BP with respect to PDAC cell mobility remains unknown. Therefore, we investigated if Gal-3BP knockdown can alter the ability of PDAC cells to adhere and migrate. We observed that Gal-3BP small interfering RNA (siRNA) transfection (Fig. 3*A*) markedly suppressed the adhesion (Fig. 3*B*), migration (Fig. 3*C*), and invasion ability of primary PDAC cells (Fig. 3*D*; additional data in *SI Appendix*, Fig. S4*A–C*). Moreover, transfection of Gal-3BP high primary PDAC cells with Gal-3BP siRNA resulted in reduced expression of epithelial-mesenchymal transition (EMT) markers, such as Zeb1, Claudin-1, and Snail (Fig. 3*E* and *SI Appendix*, Fig. S4*D–F* for additional PDC(Patient Derived Cell) data). Moreover, Gal-3BP overexpression in Gal-3BP low primary PDAC cells resulted in the upregulation of *N*-cadherin, Snail, and Zeb1 (Fig. 3*F*). To exclude the possibility that the reduced migration is caused by growth defect, we pretreated a low dose of mitomycin C (MMC) to halt cell growth and performed a transwell assay. Fig. 3*G* shows the result, indicating Gal-3BP knockdown suppresses PDAC cell migration. When two additional shRNAs targeted Gal-3BP (*SI Appendix*, Fig. S3), we found a similar antimigratory effect (*SI Appendix*, Fig. S5).

These results demonstrate that Gal-3BP positively regulates PDAC cell migration and adhesion.

Stable Knockdown of Gal-3BP Significantly Attenuates PDAC Cell Metastasis in a Mouse Model. Based on the in vitro data shown in Fig. 3, we examined the role of Gal-3BP in tumor metastasis

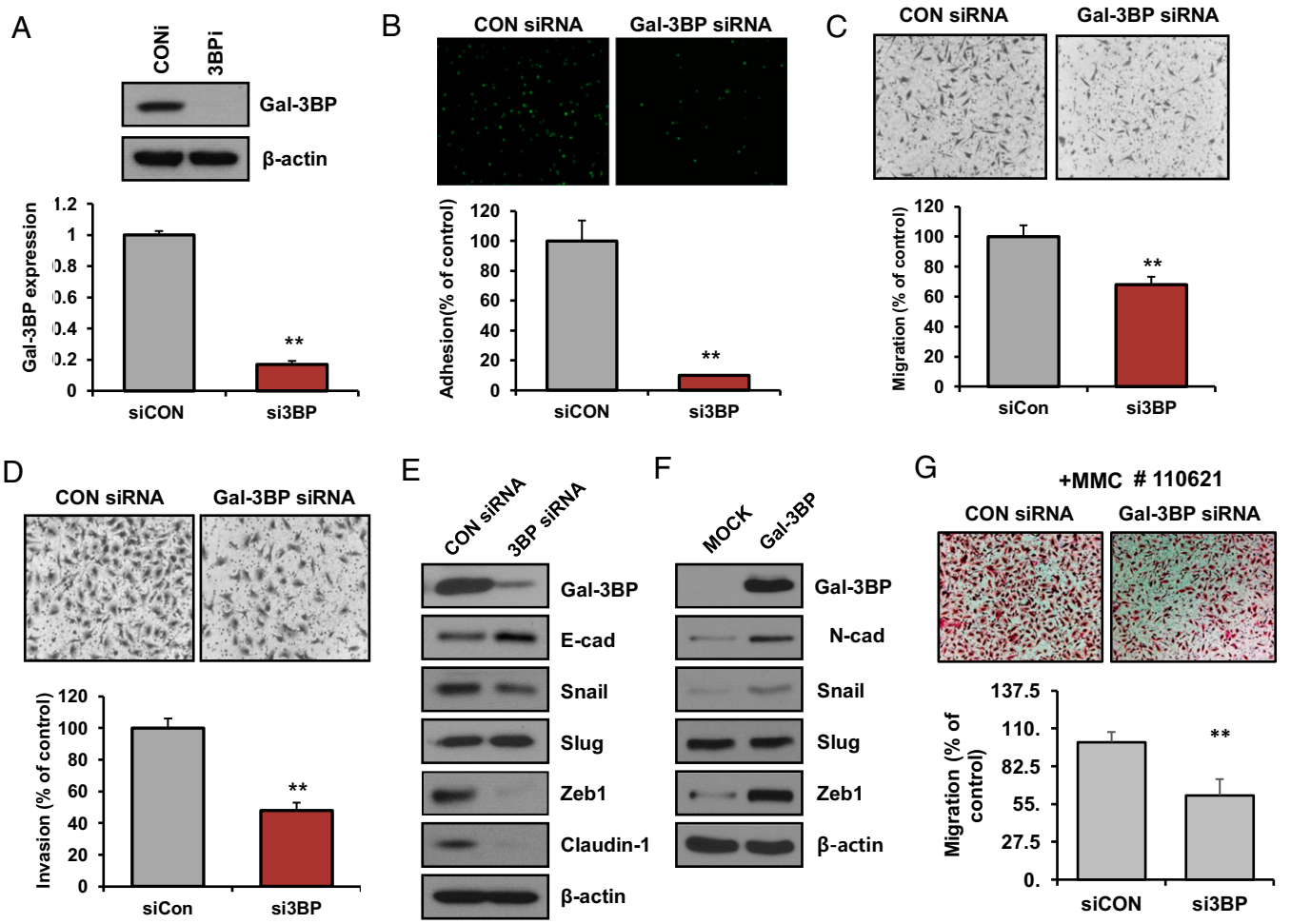

Fig. 3. Gal-3BP is required for PDAC cell attachment, migration, and invasion via the regulation of EMT markers. (*A*) mRNA and protein levels of LGALS3BP in 110621 pancreatic cancer primary cells after LGALS3BP silencing using siRNA, determined by real-time PCR and western blotting. (*B*) Adhesion assay of 110621 cells transfected with LGALS3BP siRNA (si3BP) or negative control (siCON). Representative images are shown. Bar graph indicates the adherent cell count. (*C* and *D*) Migration (*C*) and Matrigel-coated transwell invasion assay for110621 pancreatic cancer cells transfected with LGALS3BP siRNA (si3BP) or control siRNA (siCON). Representative microscopic images of cells on membrane from each group. (*E*) Western blot analysis of EMT markers from Gal-3BP high, 110621 cells with LGALS3BP knockdown. (*F*) Western blot analysis of EMT markers from Gla-3BP low, 17884 cells with LGALS3BP overexpression. See also *SI Appendix*, Figs. S4 and S5. (*G*) Migration assay results of MMC-treated 110621 cells. (*Top*) Representative images of migrated cells. Graph shows quantitation of the images (relative to control).

in vivo. Toward this, we used murine PDAC cells (PKCY(P53-Kras-Cre-YFP); a kind gift from Dr. Sung Jin Kim(Medpacto, Seoul, Korea)) isolated from LSL-Kras G12D; Trp53 R172H; Pdx1-Cre spontaneous model (31). Gal3-BP knockdown in PKCY cells (Fig. 4*A*) also resulted in reduced proliferation (Fig. 4*B*), migration (Fig. 4*C*), and EMT marker expression (Fig. 4*D*), consistent with the human PDAC data presented above. We also measured migration of PKCY cells after treatment of MMC, which showed a significant reduction in migration upon Gal-3BP knockdown (*SI Appendix*, Fig. S5*B*). In addition, two more shRNA clones of Gal-3BP consistently showed reduced proliferation and migration (*SI Appendix*, Fig. S6*A–C*). Using tail-vein injection in syngenic mouse model (in C57BL6 background), we assessed the ability of PKCY cells to form tumors in the lungs (Fig. 4*E* and *SI Appendix*, Fig. S6*D*). Lung weights (Fig. 4*F*) and nodule counts (Fig. 4*G* and *SI Appendix*, Fig. S6*E*) indicated that Gal-3BP knockdown significantly suppressed PDAC cell metastasis into lungs. The in vivo metastasis results are also validated using additional shRNA clones of PKCY (*SI Appendix*, Fig. S6*F–H*).

Gal-3BP Interacts with and Enhances EGFR Signaling in PDAC Cells. Galectin-3 activates EGFR signaling in several cancers (32–34). As EGFR is frequently upregulated and associated with poorer prognosis in PDAC (35), we examined whether EGFR activation in PDAC is affected by the upregulation of Gal-3BP, in combination with galectin-3. Indeed, p-EGFR and EGFR level is reduced upon Gal-3BP knockdown in primary PDAC cells (Fig. 5 *A*, *Left*). Conversely, secreted Gal-3BP (*SI Appendix*, Fig. S7*B*) treatment on Panc1 cells markedly increased p-EGFR levels (Fig. 5 *A*, *Right*; additional PDC data in *SI Appendix*, Fig. S7*A*). In addition, we observed reduced EGFR expression at the mRNA level (Fig. 5*B*) or protein level (Fig. 5*C*, compare first and fourth lanes of EGFR). In the presence of EGF, the time-dependent activation of EGFR was dramatically abolished in cells with stable Gal-3BP knockdown (Fig. 5*C*), indicating that Gal-3BP is a positive regulator of EGFR activation. This finding is further supported by the combinatorial treatment of two primary PDAC cell lines supplemented with secreted (*SI Appendix*, Fig. S7*B*) or recombinant Gal-3BP plus EGF, showing enhanced p-EGFR level (Fig. 5*D* and *SI Appendix*, Fig. S7*C*).

Hence, we examined how Gal3-BP affects galectin-3–mediated EGFR activation in PDAC cells. Interestingly, both combinations of EGF(E) plus galectin-3(G3) and EGF plus Gal-3BP(3BP) could enhance EGFR phosphorylation (Fig. 5*E*). Moreover, combinatorial treatment with galectin-3, EGF, and Gal-3BP

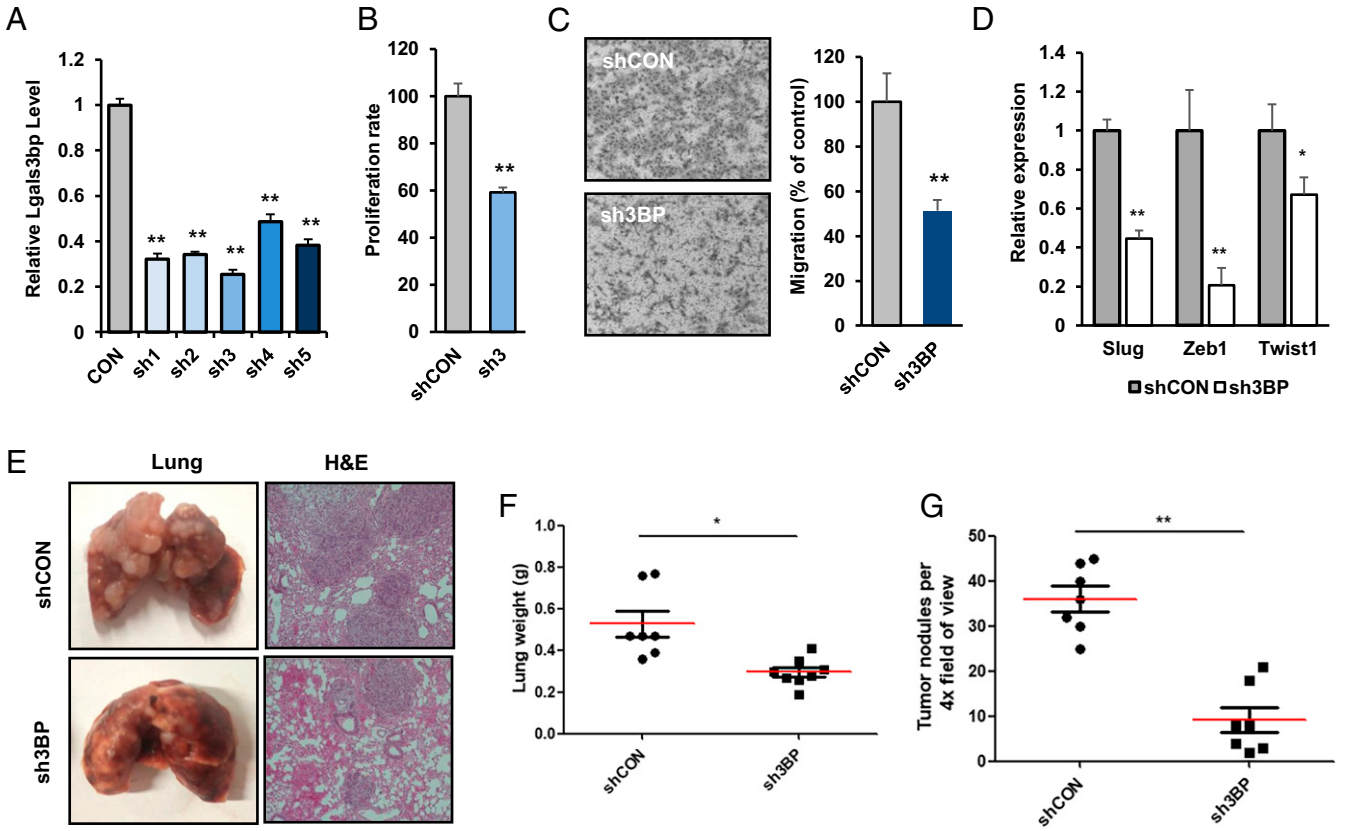

Fig. 4. Stable knockdown of Gal-3BP suppresses PDAC metastasis in mouse allograft model. (*A*) Relative level of Lgals3bp RNA in mouse PDAC cells upon shRNA mediated knockdown. (*B–D*) Reduced proliferation rate (*B*), migration (*C*), and EMT marker expression (*D*) in mouse PDAC cells after the knockdown of Gal-3BP. (*E*) Representative images of lung metastasis (*Left*) and H&E staining of lung sections (*Right*) from syngenic mice (C57BL6) injected with control (shCON) or Lgals3bp knockdown (sh3BP) cells. Scale bar: 400 μm. (*F* and *G*) Graphs depicting lung weight (*F*) and the number of metastatic lung nodules (*G*). See *SI Appendix*, Fig. S6 for additional shRNA data.

markedly enhanced p-EGFR levels (Fig. 5*E*, last lane). Further, the treatment of EGF on PDAC cells resulted in robust secretion of Gal-3BP (Fig. 5*F*) whereas the treatment with the EGFR inhibitor (EGFRi) inhibited it (Fig. 5*G*). These data suggest that a positive-feedback loop exists in the Gal3-BP–EGFR signaling. The coimmunoprecipitation analysis indicated that the Gal-3BP associated with EGFR (*SI Appendix*, Fig. S7*D*). We next examined the effect of galectin-3 (partner of Gal-3BP) knockdown on Gal-3BP–mediated EGFR activation and found galectin-3 knockdown partially inhibited the p-EGFR level, indicating that galectin-3 is also required—at least in part—for the Gal-3BP–mediated EGFR activation (Fig. 5*H*; see *Discussion*).

Gal-3BP Positively Regulates cMyc via EGFR Activation in PDAC Cells. Our data in Fig. 3 indicated that Gal-3BP is required for cellular attachment, migration, and invasion. Based on these results, we sought to identify a functional mediator that can be activated in response to EGFR signaling and that regulates such cellular events. A previous study showed that cMyc is an effector of EGFR signaling in murine pancreatic ductal epithelial cells (36). Moreover, a recent report demonstrated that cMyc alone can result in the transformation of PanIN cells into PDAC cells (37). Therefore, we investigated whether Gal-3BP regulates cMyc expression via EGFR activation. A stable knockdown of Gal-3BP (Fig. 6 *A*, *Top*) resulted in the downregulation of cMyc at the mRNA level (Fig. 6 *A*, *Bottom*). This result was further validated in another primary PDAC cell clone with transient knockdown of Gal-3BP (Fig. 6*B*). Conversely, the Gal-3BP alone or a combination of Gal-3BP and EGF upregulated cMyc (Fig. 6*C*). Consistently, the EGFRi effectively suppressed cMyc upregulation upon the Gal-3BP treatment (Fig. 6*D*), indicating that EGFR activation is necessary for the Gal-3BP–mediated cMyc activation. This result is validated in EGFR-deficient cells and generated by CRISPR-Cas9 system (*SI Appendix*, Fig. S7*E*). In EGFR-deficient cells, we observed relatively a lower level of Myc (compared to control, right panel), and it changed marginally upon EGF or Gal-3BP treatment (Fig. 6 *E*, *Right*). In addition, two tumors with stable knockdown of Gal-3BP (see Fig. 2*C*) showed reduced cMyc expression (Fig. 6*F*). Consequently, a reduced expression of several cMyc target genes was observed (*SI Appendix*, Fig. S7*E*). These data collectively indicate that Gal-3BP enhances EGFR-Myc signaling in PDAC cells. Importantly, the reduced proliferation in response to Gal3-BP knockdown (shown in Fig. 2*B*) is partially recovered upon the exogenous expression of cMyc (Fig. 6*G*), confirming that Gal-3BP–induced PDAC cell proliferation is mediated by cMyc. The reduced p-EGFR and Myc were validated in another PDAC PDC (*SI Appendix*, Fig. S7*G*). Moreover, the reduced p-EGFR and Myc expression by Gal-3BP knockdown was partially rescued by siRNA-resistant Gal-3BP expression (*SI Appendix*, Fig. S7*H*; see *Materials and Methods*), further supporting that Gal-3BP activates EGFR-Myc pathway.

Treatment with Gal-3BP Antibodies Inhibits EGFR-Myc Signaling and Metastasis of PDAC Cells in a Patient-Derived Preclinical Model. Although Gal-3BP knockdown using shRNA significantly attenuated tumor formation as well as cell migration, the shRNA approach has limitations with respect to clinical application. To develop a therapeutic agent targeting Gal-3BP, we employed an antibody phage display technique (38) to screen specific antibodies against Gal3-BP (Fig. 7*A*). Initial hit antibodies—obtained by

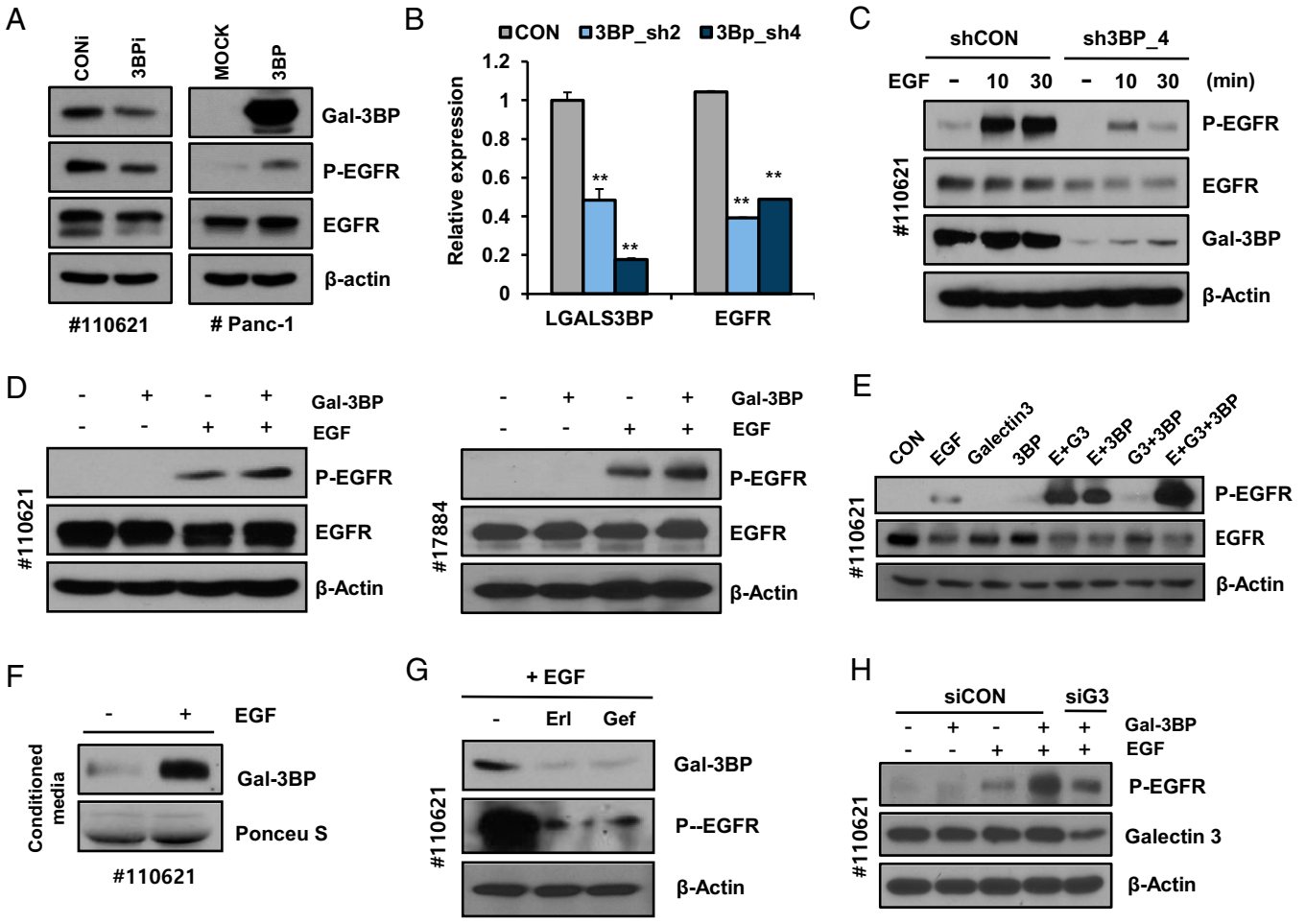

Fig. 5. Gal3-BP enhances EGFR signaling in human PDAC cells. (*A*) Gal3-BP knockdown attenuates EGFR activation. Western blotting to check for EGFR, p-EGFR, and Gal-3BP levels after siRNA-mediated knockdown of Gal-3BP in 110621 cells (*Left*) or overexpression in Panc-1 cells (*Right*). (*B*) Expression analysis of Gal3-BP and EGFR mRNA levels in two independent 110621 clonal cells (sh2 and sh4) with the stable knockdown of Gal-3BP. (*C*) Decreased phosphorylation and expression of EGFR in the background of Gal-3BP knockdown and treatment with 50 ng/mL EGF for the indicated time periods. (*D*) Gal-3BP enhances EGFR activation. Phosphorylation of EGFR was determined by western blotting in 110621 (Gal-3BP expression high cells) and 17884 (Gal-3BP expression low cells) after the combinatory treatment of Gal-3BP (250 ng/mL) and EGF (50 ng/mL). (*E*) Both galectin-3 and Gal-3BP enhance EGFR activation. Phosphorylation of EGFR was determined by western blotting after combinatorial treatment with Gal-3BP (250 ng/mL), galectin-3 (100 ng/mL), and EGF (50 ng/mL). (*F*) EGF stimulates Gal-3BP secretion. Expression analysis of secreted Gal-3BP in conditioned media by western blotting after treatment with EGF in primary (110621) cells. (*G*) Inhibition of EGFR suppresses Gal-3BP expression. Primary (110621) cells were treated with Erlotinib and Gefitinib for 2 d and then subjected to western blotting for checking the levels of Gal-3BP and p-EGFR. (*H*) Galectin-3 contributes to Gal-3BP–driven EGFR activation. Phosphoactivation of EGFR was determined after combinatorial treatment with Gal3-BP, EGF, and Gal3-BP siRNA. See *SI Appendix*, Fig. S7.

screening a Gal-3BP–immunized chicken antibody library—exhibited high affinity to recombinant Gal-3BP in vitro, as verified by enzyme-linked immunosorbent assay (ELISA). Among five candidate antibodies, we selected clones #67 and #84 owing to their inhibitory effect on cell migration (Fig. 7*B* and *SI Appendix*, Fig. S8*A*), although they did not significantly interfere with cell proliferation (*SI Appendix*, Fig. S8*B*). The antibody clones #67 and #84 were able to capture Gal-3BP, as confirmed by immunoprecipitation (Fig. 7*C*). In addition, consistent with the results of shRNA, the treatment of these two antibodies on primary PDAC cell lines showed a decreased EGFR activation and cMyc expression, although it was not as effective as siRNA-mediated gene silencing (see *Discussion*; *SI Appendix*, Fig. S8*C–F*). Moreover, we validated tumor-specific binding of the two antibody clones (Fig. 7*D* and *SI Appendix*, Fig. S9*A*), as examined by frozen section immunofluorescence (IF) of two PDAC tumors that showed no or very low expression of Gal-3BP (*SI Appendix*, Fig. S1*A*, red numbers).

Importantly, we also observed the #67 and #84 antibody clones detecting Gal-3BP in orthotopic PDAC tumor tissues both by IF (*SI Appendix*, Fig. S9*B*) and by IHC staining (*SI Appendix*, Fig. S9*C*). Based on this, we further examined the efficacy of these two Gal-3BP antibodies in the metastatic tumor model of PDAC. Human primary PDAC cells with stable luciferase expression (*SI Appendix*, Fig. S10*A*) were transplanted into mouse via tail vein, and lung tumor growth was monitored by IVIS(In Vivo optical Imaging System) imaging in conjunction with periodic antibody treatment. *SI Appendix*, Fig. S10*B* shows the changes of region of interest (ROI) signal obtained from IVIS for three groups (immunoglobulin G [IgG], #67, and #84 antibody treated) before and after anti–Gal-3BP antibody treatments. After 3 wk of treatment, we observed an overall decrease in the ROI values in the Gal-3BP-antibody–treated groups (5/7 for #67 Ab and 5/6 for #84 Ab), whereas 5/8 in control group showed increased ROI values (*SI Appendix*, Table S4 for raw data). The hematoxylin and eosin (H&E) staining of dissected lung tissue revealed nodules generated by metastasized PDAC cells, marked by the grids in Fig. 7*E*. We found that the number of nodules (Fig. 7*F*) as well as the metastatic index (measured from the area of cancer cells in the lung; Fig. 7*G*) were significantly reduced after treatment with the two Gal-3BP antibody clones. Further, another set of Gal-3BP antibody treatment

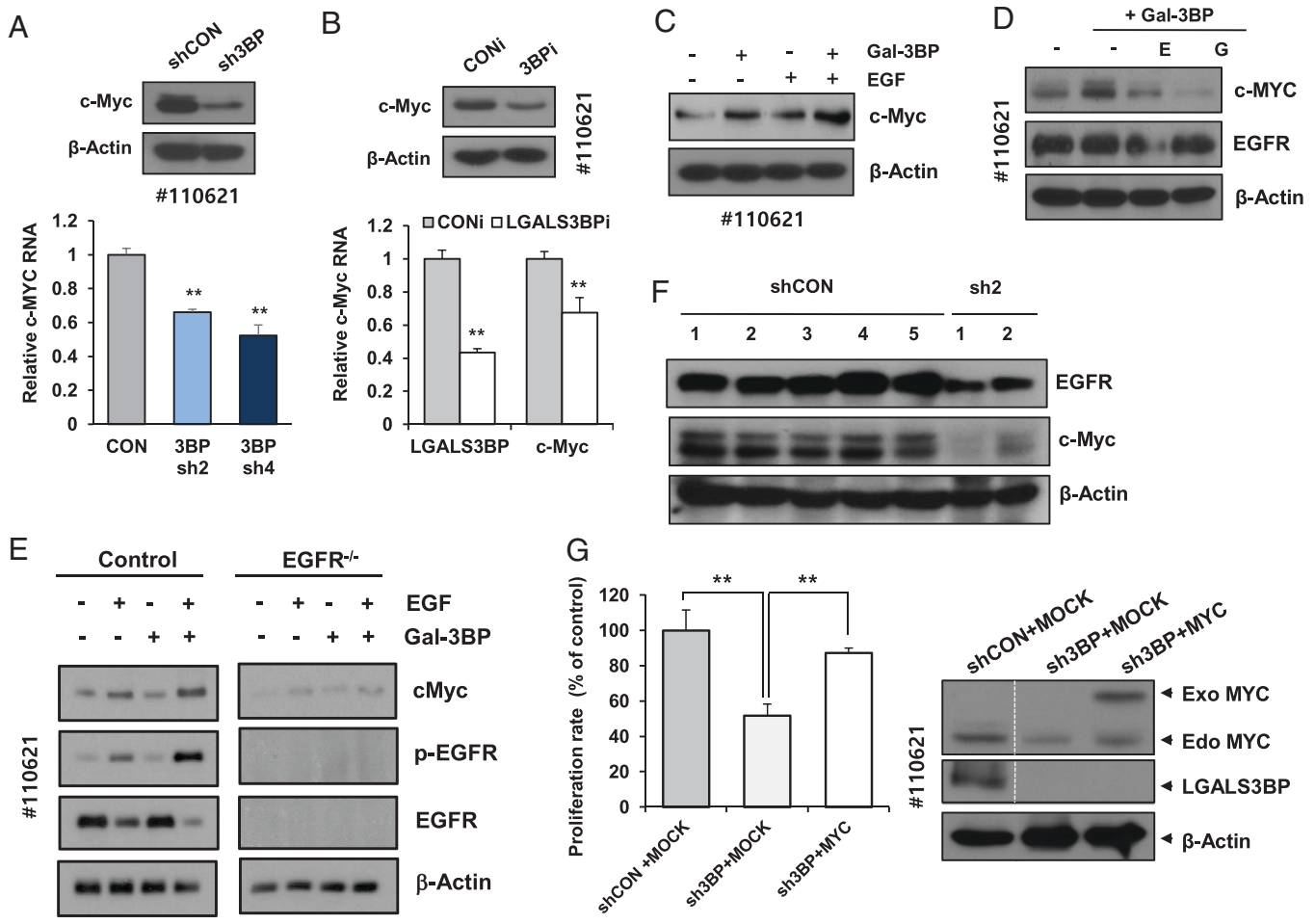

Fig. 6. cMyc mediates Gal-3BP–driven EGFR activation signal. (*A*) Reduced cMyc protein (*Top*) or RNA (*Bottom*) expression after knocking down Gal-3BP using shRNA (sh3BP). Reduced levels of cMyc mRNA were detected in two 3BP-shRNA 110621 clonal cells (sh2 and sh4). (*B*) Transient Gal-3BP knockdown attenuates cMyc expression in primary (110621) cells. (Top) cMyc protein and (Bottom) RNA levels of Gal-3BP and cMyc. (*C*) Exogenous Gal3-BP increases cMyc expression in primary (110621) cells. Cells were treated with Gal-3BP (250 ng/mL) and/or EGF (50 ng/mL) for 48 h, and the expression of cMyc was examined. (*D*) EGFRi suppresses Gal-3BP driven cMyc expression. Primary (110621) cells were pretreated with Erlotinib or Gefitinib prior to the addition of Gal-3BP. cMyc protein was detected by western blotting. (*E*) cMyc upregulation by Gal-3BP is abrogated in EGFR-deficient cells. The 110621 cells were targeted for EGFR using CRISPR-Cas9, and cMyc expression was examined after the treatment of EGF and/or Gal-3BP. (*F*) Depletion of Gal3-BP in tumor suppresses cMyc expression. Western blot analysis of EGFR and cMyc was performed in tumor lysates obtained from the mouse model shown in Fig. 2*C*. (*G*) cMyc restores PDAC proliferation attenuated upon Gal-3BP knockdown. Primary (110621) cells with Gal-3BP knockdown were transfected with empty vector (MOCK) or cMyc overexpression plasmid, and proliferation was measured. The level of cMyc protein was confirmed by western blot (*Right*) Noncontiguous blots are marked by dotted white lines.

showed a prolonged survival of PDAC tumor-bearing mouse (Fig. 7*H*; see *Materials and Methods*). These data collectively demonstrate that the blocking of Gal-3BP using specific antibodies is a good strategy to attenuate metastasis and extend survival in PDAC preclinical model (summarized in graphical abstract).

Discussion

A major obstacle in the identification of a drug target or tumor biomarker using the patient samples is the variability across donors, including genetic diversity, lifestyle, disease state, and therapeutic history of each patient (39). To overcome this, a large number of specimens as well as precise statistical analysis is needed, but this not always possible in pancreatic cancer research (40). In this respect, the PDX model serves as an effective preclinical model, wherein most of the host variables are controllable, and an ideal control (ungrafted littermates) can be easily obtained (41). Therefore, despite the known limitations, such as a compromised immune environment (42), the PDX model enables us to design a simple (with a small number of mice), rapid screening strategy for the identification of protein biomarkers or therapeutic targets. Further, a dilution effect as well as the intrinsic low-level expression of the tumor-originated secreted protein makes the identification of blood biomarkers difficult (43). To circumvent this limitation, we introduced the analysis of TIF and managed to improve the detection of the candidate marker proteins.

The interaction of EGF with EGFR and its activation is well characterized (44). However, despite its critical role in tumorigenesis, not much is known about EGFR-binding proteins (other than EGFR). The STRING (Search Tool for the Retrieval of Interacting Genes/Proteins) database (45) shows ~10 protein interactions, but most of them are adaptors or kinases that transmit the activation signal in the cytoplasmic domain (*SI Appendix*, Fig. S10*D*). In this respect, characterization of EGFR activating protein contributes to the understanding of EGFR activation as well as to designing a therapeutic target. Galectin-3 has been shown to activate EGFR in pancreatic cancer (34) and other cancer types (46, 47). In parallel with the recent progress on the galectin-3 antagonist (48, 49), we demonstrate here that anti–Gal-3BP antibody is an alternative for effectively blocking the activation of EGFR in PDAC. Despite this, we also need to consider that galectin-3 has multiple

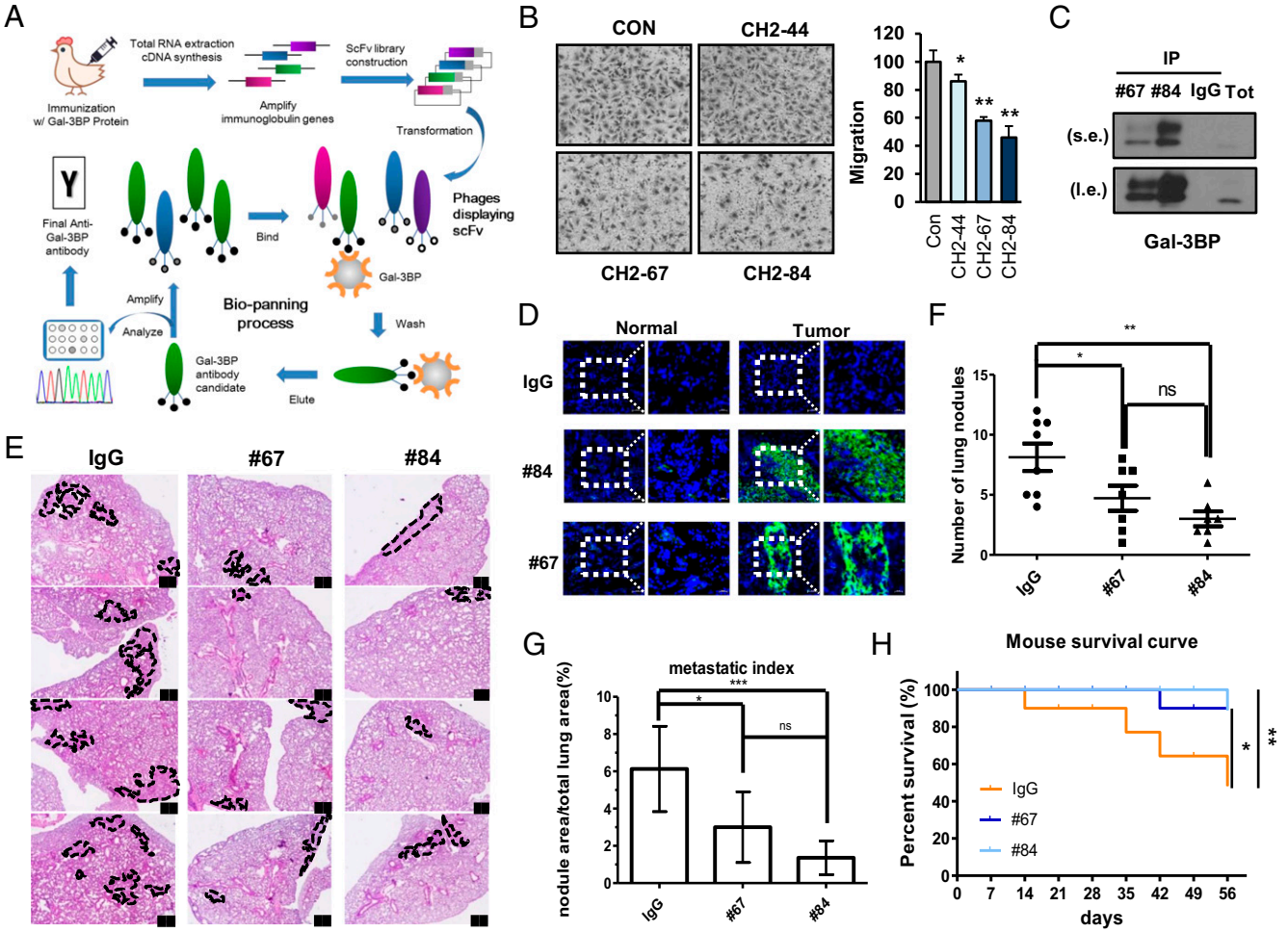

Fig. 7. Anti–Gal-3BP antibody isolated by phage display attenuates migration of PDAC cells and metastasis in patient-derived preclinical model. (*A*) Schematic diagram depicting the Gal3-3BP antibody screening by phage display technique. (*B*) Inhibitory effect of Gal3-3BP antibody (CH2-44, CH2-67, CH2-84) on pancreatic cancer cells (110621) migration. Representative image of migration (*Left*) and its quantitation (*Right*) are shown. (*C*) Immunoprecipitation followed by western blot demonstrated that two antibody clones (#67 and #84) bind with Gal3-BP. Cells treated with IgG were used as a negative control. (*D*). Specific binding of anti–Gal-3BP antibodies (#67 and #84) on primary PDAC. The #6 sample of PDAC used in *SI Appendix*, Fig. S1*A* was used for IF of Gal-3BP. Dotted area indicates magnified region shown aside. (*E*) Representative H&E staining of lung sections. Metastasized tumor regions are marked by black-dotted grids; scale bar: 200 μM. (*F*) A graph showing the nodule count from lung sections obtained from mice injected with primary PDAC cells and treated by antibodies (IgG, #67, and #84; $n = 22$). (*G*) A graph showing metastatic index, indicating the area occupied by tumor cells in each lung ($n = 22$). (*H*) Survival curve of the mouse in lung metastasis model, treated with IgG or anti–Gal-3BP antibodies. See *Materials and Methods* for details.

binding partners (50) other than EGFR. Given Gal-3BP can preferentially interact with galectin-3, the impact of Gal-3BP can be diverse. Indeed, when we analyze proteome after treatment of Gal-3BP in comparison with EGF (*SI Appendix*, Fig. S11), we found ∼50 Gal-3BP–specific protein changes. This upregulation was reversed by #84 anti–Gal-3BP antibody treatment (*SI Appendix*, Fig. S11, last column in heatmap). Hence, we cannot exclude that the antimetastatic effect of Gal-3BP antibody is attributed to multiple signal pathways.

Although we have successfully developed antibodies against Gal-3BP and demonstrated their antitumor effect in a mouse model, several points need to be considered in order to translate this into a therapeutic agent for cancer patients. Firstly, recent reports indicated a multifunctional role of Gal-3BP not only in cancer, but also in innate immunity function (51). In the report, Gal-3BP is induced in response to viral and bacterial infection and regulates cytokine production/secretion, viral assembly, and lipopolysaccharide response (52). Therefore, selective delivery method to tumor site or an appropriate dosage of anti–Gal-3BP antibody should be predetermined in order to prevent adverse antiimmune function. Secondly, the effect of Gal-3BP knockdown on metastasis (Fig. 4 *E*–*G*) could be the combination of proliferation (Fig. 4*B*) and migration effect (Fig. 4*C*). Even though we provided migration data after MMC treatment (to hold cell proliferation), the antimetastatic effect of Gal-3BP blockade should not be overestimated. Lastly, compared to EGFRi, we need to clarify the pros and cons when we use anti–Gal-3BP antibody. To obtain an overview for this question, we performed comparative proteomic analysis between EGFRi and anti–Gal-3BP antibody treatment (*SI Appendix*, Fig. S12). We observed that quite a large portion of protein upregulation by EGF+Gal-3BP is reversed by either EGFRi or anti–Gal-3BP Ab (*SI Appendix*, Fig. S12*A*, group C2). However, we also observed that the expression of a subgroup of C2 (∼30 proteins) is not reversed by EGFRi. Similarly, we found the expression of a subgroup of C6 (∼50 proteins) is reversed by EGFRi, but not by anti–Gal-3BP Ab (*SI Appendix*, Fig. S12*B*). Further study on these proteomic changes upn anti-Gal-3BP Ab treatment will allow us to understand the molecular impact of the Gal-3BP blockade.

Despite these limitations, we propose the Gal-3BP antibody as a promising therapeutic agent, since it effectively attenuated the metastasis of PDAC cells in our mouse model. One of the major challenges in pancreatic cancer is its highly metastatic

nature, which restricts the resectable tumor to 15 to 25% upon diagnosis (53). Therefore, in addition to early detection, identifying a therapeutic option to prevent or suppress metastasis is critical for the management of pancreatic cancer. Several potential antimetastatic agents, including matrix metalloproteinase inhibitor (54), JG243 (HIF-1a inhibitor; ref. 55), JQ1 (vasculogenic mimicry inhibitor; ref. 56), AZD6244 (MEK inhibitor) with BMS833923 (Hh inhibitor; ref. 57), and Metavert (GSK3B and HDAC inhibitor; ref. 58) have been identified. Future studies should focus on combinatorial therapy with Gal-3BP antibody and these antimetastatic agents as well as a promising combination with immunotherapy (59, 60), which will broaden the options available for enhancing the survival of PDAC patients.

Materials and Methods

Ethical Guidelines and Human Sample Acquisition. Human PDAC specimens were obtained and deidentified with permission from the institutional review board of the Asan Medical Center (S2013-0744-0009). Protocols for animal experimentation were reviewed and approved by the Institutional Animal Care and Use Committees of Asan Institute for Life Sciences (AILS, Project Number: 2015-12-164). All mice were maintained in the specific pathogen–free facility of the Laboratory of Animal Research at AILS (Seoul, South Korea). For survival curve of the antibody treatment, we sacrificed mouse when the body weight decreased by more than 20% of the initial value, according to ethics regulation of AILS. The biospecimen and data used in this study were provided by Asan Bio-Resource Center, Korea Biobank Network (2020-20(217)).

Cell Culture and Transfection. Human pancreatic cancer cell lines were maintained in Dulbecco's modified Eagle's medium (DMEM) supplemented with 10% fetal bovine serum (FBS) and 1% penicillin/streptomycin. Primary pancreatic cancer cells were cultured in RPMI (Roswell Park Memorial Institute) supplemented with 5% FBS, 1% penicillin/streptomycin, 20 ng/mL EGF, 4 μg/mL hydrocortisone, and 4 μg/mL transferrin. HPDE cells were cultured in keratinocyte serum-free medium supplemented with EGF and bovine pituitary extract (Invitrogen). All cells were cultured at 37 °C in an atmosphere containing 5% CO_2. Cells were transfected with control siRNA or LGALS3BP siRNA using Lipofectamine 2000 (Invitrogen). LGALS3BP siRNA was designed by Genolution Inc. and had the following sequence: 5′-CGCACCAUUGCCUACGAAAUU-3′.

Primary culture. Primary cancer cells were isolated from tumors derived from PDX models. Fresh tumor tissue was minced into 1- to 2-mm pieces using sterile scissors, scalpel, and forceps. For tissue digestion, the tissue pieces were placed in a 15-mL conical tube containing 3 to 5 mL RPMI medium 1640 (PAN, DEU) supplemented with 5% FBS (PAN, AUS), 1% penicillin/streptomycin (HyClone, United States), 20 μg/mL collagenase type III (Sigma Aldrich, United States), and 840 ng/mL Fungizone (Gibco, United States) and incubated on a shaking incubator at 37 °C for 2 h. Following incubation, the digested tissue pieces were washed with RPMI medium 1640 and centrifuged at 800 rpm for 3 min (×3). The tissues were placed in a collagen-coated T25 flask and cultured using RPMI medium 1640 supplemented with 5% FBS, 1% penicillin/streptomycin, 20 ng/mL hEGF (Gibco, United States), 4 μg/mL hydrocortisone (Sigma Aldrich, United States), 4 μg/mL transferrin (Sigma Aldrich, United States), and 840 ng/mL Fungizone at 37 °C in an atmosphere containing 5% CO_2. After 2 to 4 d of incubation, cells started to attach to the collagen-coated surface of the T25 flask.

Antibodies and Reagents. Cells were lysed in RIPA buffer containing protease and phosphatase inhibitors. Lysates were centrifuged at 14,000 rpm for 15 min, and the supernatant was collected. Subsequently, the proteins were separated via sodium dodecyl sulfate (SDS)–polyacrylamide gel electrophoresis. Immunoblotting was performed using antibodies against LGALS3BP (R&D systems), p-EGFR (cell signaling), EGFR (cell signaling), CA19-9 (Abcam), and β-actin (Santa Cruz Biotechnology).

shRNA-Mediated Knockdown of Gal-3BP. Plasmids targeting containing shRNA against human and mouse LGALS3BP were purchased from Sigma Aldrich: human LGALS3BP (#1 TRCN0000029418; #2 TRCN0000372778; #3 TRCN0000029417; #4 TRCN0000372838; #5 TRCN0000029414) and mouse LGALS3BP (#1 TRCN0000325878; #2 TRCN0000066333; #3 TRCN0000066334; #4 TRCN0000066336; #5 TRCN0000066335). In order to generate recombinant lentiviruses, HEK293T cells were cotransfected with a lentiviral expression vector and lentiviral packaging vectors (VSVG and PAX2) using Lipofectamine 3000 (Invitrogen, Camarillo, CA). Subsequently, the supernatants were collected twice at intervals of 1 d. For transduction of 110621 or PKCY cells, lentiviruses were included in the culture medium for 2 d. Finally, to select cells with a stable knockdown, a selection pressure was applied by using puromycin (1 μg/mL) or puromycin (2 μg/mL).

Generation of siRNA-Resistant, Wobble Mutant Gal3BP Expression Vector. Mutant recombinant Gal3BP vector was generated by site-directed mutagenesis in the shRNA seed match region of the Gal3BP CDS(Coding Sequence) . In the mutant Gal3BP vector, 8 nt of the shRNA sequence targeting the CDS region (AGGACAATCGCTTATGAG of the mutant Gal3BP CDS region) were mutagenized using the KOD-Plus-Mutagenesis kit (TOYOBO, Japan), according to the manufacturer's instruction. The sequence of mutant primers are as follows: Gal3BP_siMut_Forward 5′-GTCTGGCGGCTCAGATAGGACAATCGCTTATG AGAACAAAGCCCTGATGC -3′; Gal3BP_siMut_Reverse 5′-GCATCAGGGCTTTGTTCT CATAAGCGATTGTCCTATCTGAGCCGCCAGAC-3′.

Migration, Invasion, and Proliferation Assays. The migration and invasion abilities of the cells were assayed by using transwell chambers (Corning Costar) and Matrigel-coated chambers containing 6.5-mm–diameter polycarbonate filters (8-μm pore size). The cells were trypsinized and suspended at a final density of 1×10^6 cells/mL in serum-free medium. Subsequently, 100 μL of the cell suspension was loaded into each of the upper wells, and culture medium supplemented with serum was added to the plate as a chemoattractant. The chamber was incubated at 37 °C for 24 h. Following this, the cells were fixed and stained with H&E. Nonmigrated cells in the upper chamber were removed using a cotton swab. The number of migrated and invaded cells was quantified by manual counting under an optical microscope (×200). Cell viability was evaluated using Ezcytox according to the manufacturer's protocol. Cells were seeded at a density of 2×10^3 cells/100 μL in each well of a 96-well plate and incubated at 37 °C for 72 h. The absorbance of the wells was measured at 450 nm using a Molecular Devices microplate reader, with a reference wavelength of 650 nm.

IHC Analysis. Fresh specimens were immersed in 10% formalin for 4 d and subsequently embedded in paraffin. Paraffin sections (4 μm thick) were deparaffinized using xylene and rehydrated by treatment with graded alcohols. Endogenous peroxidase activity was blocked using 3% hydrogen peroxide prepared in methanol for 20 min. Antigen retrieval was performed via heat treatment in Tris-EDTA buffer (Abcam) for 20 min, followed by incubation with 3% normal goat serum for 20 min to block nonspecific binding. After blocking, the sections were incubated with Ki67 antibody (Abcam, 1:50) diluted in 1% normal goat serum at 4 °C overnight. Sections were rinsed in phosphate-buffered saline (PBS) and incubated with HRP(Horse Radish Peroxidase)-conjugated secondary antibody (1:200) at room temperature for 1 h. Finally, the sections were developed using diaminobenzidine (Thermo Scientific) and counterstained with hematoxylin. The samples were mounted with coverslips using Permount (Fisher Scientific), and the sections were observed under a light microscope. Analysis was performed using Image J.

IF Staining of PDX Tissues. PDX samples for IF staining were embedded into OCT(Optimal Cutting Temperature) compound and stored at −80 °C deep freezer until ready for sectioning. The samples were cut into 5-μm sections on a cryostat. IF staining was performed according to the manufacturer's instructions (R&D system, Minneapolis, MN). In brief, tissues were incubated overnight at 4 °C with primary antibodies: Gal-3BP (1 μg/mL, R&D systems, Minneapolis, MN) and Gal-3BP #84 and #67 (1 ug/mL, custom mouse monoclonal antibodies, Asan Medical Center Core). Tissue was then stained with 1:1,000-diluted secondary antibodies, donkey anti-goat Alexa Fluor 488 (Invitrogen, Thermo Fisher Scientific, Waltham, MA), and goat anti-mouse Alexa Fluor 488 (Invitrogen). Images were captured using a LMS710 confocal microscope (ZEISS, Jena, Germany) and analyzed using Image ZEN black edition (ZEISS).

IF Staining of Primary Tumors. PDAC ($n = 10$) and matched normal pancreas ($n = 10$) tissue samples were collected from 10 patients receiving a

pancreatectomy. The tissue specimens were obtained during the surgery and immediately cut into pieces. Patient PDAC or PDX samples for IF staining were embedded into OCT and stored at −80 °C deep freezer until ready for sectioning. The samples were cut into 5-μm sections on a cryostat. IF staining was performed according to the manufacturer's instructions (R&D system, Minneapolis, MN). In brief, tissues were incubated overnight at 4 °C with primary antibodies: Gal-3BP (1 μg/mL, R&D systems, Minneapolis, MN) and Gal-3BP #84 and #67 (1 ug/mL, custom mouse monoclonal antibodies, Asan Medical Center Core). The remaining procedures are the same as the above section.

Generation of CRISPR/Cas9-based EGFR KO cells. Lentiviral guide RNA plasmids (pLKO.sgRNA.EFS.tRFP) were purchased from Addgene (Plasmid, #57823). Two sgRNA (small guide RNA) were designed for EGRF and were inserted into the vector using BsmB I. The sgRNA sequences (5′ to 3′) targeting EGFR (Exon12, GGGTCCCTGACGCAGAGAAC
GGCCTTACAGTCGGCCTTACAGTCGGCTCCGTCCCTT, Exon14, GAAAACAACACCCTGGTCTG-GAAGTACGCAGACGCCGGCCATGTG) were as follows: sgRNA1, CCCAGGGACTGCGTCTC TTGCCGGAATGTCAGCCGAGGC AGGGAA, sgRNA2, CTTTTGTTGTGGGACCAGACCTTCATGC GTCTGCGGCCGGTA CAC.

The lentiviral production was performed following the manufacturer's instructions. LentiCas9-Blast (Addgene, #82372) or pLKO.sgRNA.EFS.tRFP (Addgene, #57823) was cotransfected with packaging plasmids pMD2.G and psPAX2 into HEK293 cells using Lipofectamine 2000 (Invitrogen, CA). After 48 h, the lentiviral particles were harvested and infected into PDX cells (110621). For the stable Cas9-expressing cells, the cells were treated with 4 ∼ 8 μg/mL Blasticidin S hydrochloride (Sigma). To examine cMyc expression by EGFR knockout, the Cas9-expressing cells were infected with lentiviruses expressing either control (pLKO5-tRFP; Addgene 57823) or sgRNAs (pLKO5-sgRNAs-tRFP). After 48 h, the cells were incubated with Gal-3BP (250 ng/mL, 1 h) and EGF (50 ng/mL, 30 min).

In vivo tumor formation and imaging. Cells (110621 cell line) were resuspended in 100 μL PBS at a density of 2×10^6 and injected into the dorsal flank of 6- to 8-wk-old male BALB/c nude mice. Tumor growth was monitored, and tumor volume was measured using calipers. Tumor size (mm^3) = L (length) × W^2 (width)/2. Subcutaneous tumors were excised and weighed. Subsequently, tumor tissues were fixed in formalin, embedded in paraffin, and then stained with H&E. IHC was performed to check the expression of K_i-67, which is a marker of proliferating cells, and the number of positively stained cells was calculated by counting the number of immune-positive cells in five selected fields under a microscope.

TMA Analysis. PDAC for TMA were collected from Asan Medical Center tissue cores (Seoul, South Korea). Tissue blocks and their matching H&E–stained slides were retrieved and confirmed by a pathologist to identify representative tumor regions. PDAC ($n = 153$) or matched normal pancreas ($n = 21$) were sampled from representative areas using a 2.0-mm punch. For Galetin-3BP IHC staining, paraffin-embedded samples were cut 4-μm sections and incubated with primary antibodies against Gal-3BP (1:100, Solarbio Life Sciences, Beijing, China) and Gal-3BP #84 and #67 (10 μg/mL, custom mouse monoclonal antibodies, Asan Medical Center Core) overnight. Images were taken using a digital camera DP27 (Olympus, Shinjuku, Japan) coupled to an Olympus BX53 Upright Microscope (Olympus). Images were analyzed by Olympus CellSens Standard software. Based on the amount of Gal-3BP–positive cells, the tumor speciem were subdivided into four categories as follows: 0, 10%; 1, 11 to 30%; 2, 30 to 50%; and 3, >50% positive cells. Semiquantative intensity was scored as 0 (negative), 1 (weak), 2 (moderate), and 3 (strong) (Fig. 1*G*).

TIF Isolation and Proteomic Analysis. Tumor tissues weighing 0.25 g were cut into small pieces (1 to 3 mm^3) and carefully washed in 3 mL PBS. Tumor samples were subsequently transferred to 1.5-mL tubes and incubated at 37 °C for 1 h in 1 mL PBS in a humidified CO_2 incubator. The samples were then centrifuged, and the supernatant was collected. The LC-MS/MS analysis of the tumor secretome was described previously (61).

Protein Digestion and TMT Labeling. Seven cell samples were suspended in lysis buffer (5% SDS, 50 mM triethylammonium bicarbonate [TEAB], 1× Halt protease inhibitor mixture [Cat. No.: 78429; Thermo Fisher Scientific, Waltham, MA] pH 8.5); lysed for 1 min with the probe sonicator (VCX-130; Sonics and Materials Inc., Newtown, CT) at an amplitude of 28% in pulse mode (1 s on/2 s off); and centrifuged at 18,000 × g for 10 min at 4 °C. The protein concentration of each supernatant containing extracted proteins was measured with a BCA(Bicinchoninic Acid) protein quantification kit (Pierce BCA Protein Assay Kit; Cat. No.: 23225; Thermo Fisher Scientific, Waltham, MA). To a 300-μg aliquot of proteins was added dithiothreitol to a final concentration of 20 mM for 10 min at 95 °C to reduce disulfide bonds. Reduced samples were then incubated with 40 mM iodoacetamide for 30 min at room temperature in the dark. By a 10-fold dilution of 12% phosphoric acid, acidified samples were loaded onto suspension-trapping (S-Trap) mini columns (ProtiFi, Farmingdale, NY; Cat. No.: CO_2-mini-80). We treated S-trap proteolysis according to the manufacturer's protocol, followed by the addition of 12 μg Lys-C/trypsin mixture (Promega Corp., Madison, WI; Cat. No.: V5071) and incubation for 16 h at 37 °C. The eluted peptide mixture was lyophilized using a cold trap and stored at −80 °C until use. Before tandem mass tag (TMT) 7-plex labeling, dried peptide samples were reconstituted in 0.1% formic acid, and the total peptide concentrations were measured using a UV/Vis spectrophotometer (NanoDrop One, Thermo Fisher Scientific) at a wavelength of 280 nm, with the sample type option set to "1 Abs = 1 mg/mL." In total, 100 μg peptide per sample was mixed with TMT reagent (Thermo Fisher Scientific) and mixed according to the manufacturer's protocol.

Basic pH Reversed-Phase Fractionation. TMT 7-plex labeled peptide mixture was injected into a 100-μL sample loop with XBridge C-18 column (4.6-mm i.d. × 250-mm length; pore size 130 Å and particle size 5 μm; Waters Corporation, Milford, MA) on a binary HPLC(High Performance Liquid Chromatography) system (20A Prominence, Shimadzu, Tokyo, Japan). The fractionations were performed at a flow rate of 0.5 mL min^{-1}. We used 10 mM TEAB (pH 8.5) as mobile phase A and 10 mM TEAB in 90% acetonitrile (pH 8.5) as mobile phase B. Gradients of 5 to 5% B for 8 min, 5 to 40% B for 57 min, 40 to 44% B for 6 min, 44 to 60% B for 15 min, 60 to 60% B for 6 min, 60 to 5% B for 2 min, and 5 to 5% B for 30 min were applied. After 8 minutes of LC run, 24 cycles of receiving from eight fractions sequentially by 0.45 mL each.

LC-MS/MS. Eight fractionated peptides were separated using the Dionex UltiMate 3000 RSLCnano system (Thermo Fisher Scientific). Each dried sample was reconstituted with 500 μL 0.1% formic acid and a 5-μL aliquot, which was injected into a C18 Pepmap trap column (20 mm × 100 μm i.d., 5 μm, 100 Å; Thermo Fisher Scientific) and separated by an Acclaim Pepmap 100 C18 column (500 mm × 75 μm i.d., 3 μm, 100 Å; Thermo Fisher Scientific) over 200 min (250 nL/min) using a 0 to 48% acetonitrile gradient in 0.1% formic acid and 5% dimethyl sulfoxide for 150 min at 50 °C and measured in triplicate. The LC column was coupled to a Q Exactive MS (Thermo Fisher Scientific) with a nano-ESI(Electrospray ionization) source (2,500 V in positive ion mode). MS settings included MS1 scans (70,000 resolution, 350 to 1800 m/z scan range, 3×10^6 AGC(Automatic Gain Control), and 50 ms maximal ion time) and 20 data-dependent MS2 scans (35,000 resolution, starting from 120 m/z, 200 to 2,000 m/z scan range, 1×10^5 AGC, 120 ms maximal ion time, 1.2 m/z isolation window, HCD(Higher-Energy Collisional Dissociation), 32 specified normalized collision energy [NCE], and 20 s dynamic exclusion).

Proteomic Identification and Quantification. The acquired MS/MS spectra were retrieved on the SequestHT on Proteome discoverer (version 2.4; Thermo Fisher Scientific) and compared with the SwissProt human protein sequence database (March 2021). Precursor mass tolerance was set to ±10 ppm, and MS/MS tolerance was set at 0.02 Da. The search parameters were set to default parameters, including cysteine carbamidomethylation and lysine TMT6plex as a fixed modification and N-terminal TMT6plex and acetylation and methionine oxidation as variable modifications with two miscleavages. False discovery rates (FDRs) were set at 1% for each analysis using "percolator." The reporter ion quantification was calculated by signal-to-noise ratio values or intensity. Protein abundance was estimated using quantified unique peptides.

Statistical Analysis for Proteome Data. Raw reporter ion intensities for the average number of technical replications for each channel were log2-transformed and normalized by width adjustment. Sample groups were compared by ANOVA tests with FDR correction using Perseus software (version 1.6.15.0). After protein-wise z-score substitutions, hierarchical clustering was performed on proteins for Euclidean distance with complete linkage and samples based on Spearman's rank correlation.

MRM Method Establishment for LGAL Quantification. Representative tryptic peptide for Gal3BP was determined to be ELSEALGQIFDSQR (molecular weight: 1591.78 Da, 2+ charged) after PeptideAltas (www.peptideatlas.org/) search. For MRM method establishment, stable isotope-labeled internal standard (SIS) peptide for ELSEALGQIFDSQR (molecular weight: 1601.81 Da, 2+ charged) was synthesized using heavy isotope labeled lysine at C-terminal (L -*Lysine*-13C6,15N2) with 95% purity (Peptron, South Korea). To generate a list of possible b- and y-series product ions for doubly charged peptide of ELSEALGQIFDSQR, Skyline software (64 bits, version 19.1.0.193, University of Washington, MacCoss Lab) was used at the m/z range from 300 to 1,400. In brief, peptide sequence was imported into Skyline in FASTA format and designed into light peptide and SIS peptides with a list of fragment ions. Exported transitions from Skyline was used to optimize CE and retention time determination with default instrument parameters. MRM was performed using triple quadrupole MS with a jet stream ESI source (6495 Agilent, Agilent Technologies, Santa Clara, CA) coupled with HPLC system (1290 Infinity, Agilent Technologies, Santa Clara, CA). A mixture of light peptide and SIS peptide was injected directly into a reversed-phase analytical column (Zorbax Eclipse Plus C18 rapid resolution HD, 2.1 × 100 mm, 1.8-μm column [Agilent Technologies]) with 40 °C oven temperature. The peptide samples were separated and eluted at 0.3 mL/min on a linear gradient of mobile phase B from 5 to 30% B in 19 min (mobile phase A: water/0.1% FA (Formic Acid); mobile phase B: acetonitrile/0.1% FA). The gradient was ramped to 70% B for 3 min and ramped to 90% for 3 min and 5% B for 10 min to equilibrate the column for the next run. The total LC run time was 35 min. After the initial MRM run using theoretical transition list from Skyline, the top five most intense transitions for the light peptide and SIS peptide were selected for CE optimization and retention time determination, respectively. Targeted MS acquisitions were performed using 4-min detection windows, a 100-ms cycle time using the dynamic MRM method (*SI Appendix*, Table S1). The source settings were set as below: gas temperature was 250 °C, gas flow was 15 L/min, nebulizer was 30 psi, sheath gas temperature was 350 °C, sheath gas flow was 10 L/min, capillary was 3500 V for positive ion funneling, nozzle voltage was 300 V, and iFunnel parameters for high-pressure RF(Radio Frequency) were 90 V and low-pressure RF were 60 V. To maximize assay sensitivity, the CE used to fragment light and SIS peptide ions was optimized. In detail, the default linear equation was used to predict the optimal CE for each fragment ion in Skyline software with step size to 1 (5 V on each side of the predicted CE, incremental at 1 V). The CE that showed the highest peak area for each transition was used for final methods development. Five transitions for light peptide and SIS peptide were selected for subsequent MRM analysis. To determine the response curve, MRM was performed using eight points of concentration samples ranging from 0 to 500 fmol with blank plasma matrix. Limit of detection and limit of quantitation were determined as previously described (PMID: 19596694).

Quantification of Plasma LGAL Using MRM. In total, 14 high-abundant plasma proteins (albumin, IgG, haptoglobin,) in 40 ul plasma were depleted using MARS-h14 column (Agilent), and low-abundant protein fraction was denatured using 5% SDS buffer and digested via S-trap mini platform following the manufacturer's protocol (Profiti, United States) using trypsin/LysC protease (Cat. No.: C5071, Promega, United States) (PMID: 29754492). The eluted peptide mixture was dried and reconstituted using 0.1% FA to be 1 ug/ul. The SIS peptide was spiked to be 50 fmol, and targeted MRM analysis was performed using established MRM methods. Quantity information for each transition was extracted using Skyline, and the concentration of plasma LGAL was calculated using peak area of 50 fmol SIS peptide.

Phage Display for the Gal-3BP Antibody Screening. Three white leghorn chickens were immunized and boosted thrice with the recombinant Gal-3BP produced in house. Chickens were euthanized a week after receiving the third booster dose, and their spleens as well as bone marrows were harvested for total RNA isolation using TRIzol Reagent (Thermo Fisher Scientific). Complementary DNA (cDNA) was synthesized using SuperScript IV First-Strand Synthesis System (Thermo Fisher Scientific), according to the manufacturer's protocol. Using cDNA as a template, the genes encoding the variable regions of heavy and light chains were amplified and used for the construction of a chicken scFv-displayed phage library, as previously described (62). The chicken scFv-displayed phage libraries were subjected to four rounds of biopanning against Gal-3BP, in accordance with the existing protocols (63). The nucleotide sequences of the reactive scFv clones were determined by Sanger sequencing (Cosmogenetech, Seoul, Korea).

Antibody Treatment of Mouse Model of PDAC with Lung Metastasis. Ten-week-old immunodeficient NRG (NOD/RAG1/2$^{-/-}$IL2Rγ$^{-/-}$) male mice were obtained from Jung-A Bio Laboratories (Osong, South Korea). For the lung metastasis model, a primary pancreatic cancer cell line (110621) with stable luciferase expression was used. The primary PDAC cells with luciferase expression were generated by transfecting with retroviral vector (pMXs-IRES-Puro Retroviral Vector, RTV-014) obtained from a packaging cell line (Platinum-A Retroviral Packaging Cell Line, Amphotropic, RV-102). The cells were resuspended at a density of 2×10^5 cells/100 μl in Matrigel (Corning Matrigel Matrix from Corning Life Sciences) and injected into the tail vein. One week after surgery, the luciferase signal in the tumor was monitored using the IVIS Spectrum In Vivo Imaging System (Perkin-Elmer). Antibody treatment was performed in the following three groups: IgG-treated control ($n = 4$), #67 antibody-clone–treated ($n = 6$), and #84 antibody-clone–treated ($n = 6$). The antibodies were intravenously injected (200 μL; 1 mg/mL) once a week. After four injections, the mice were euthanized, and tumors were analyzed.

Statistics. All data are presented as mean ± SE. The comparisons between two groups were performed using Student's *t* test, and comparisons among multiple groups were performed using ANOVA. $^*P < 0.05$, $^{**}P < 0.01$, and $^{***}P < 0.001$.

Data Availability. All study data are included in the article and/or *SI Appendix*.

ACKNOWLEDGMENTS. This study is supported by the Korean Health Technology R&D Project, Ministry of Health & Welfare, Republic of Korea (Grants HI14C2640 and HR21C0198030021) and by the AILS (Grant 2021IP0022-1).

1. S. Chandana, H. M. Babiker, D. Mahadevan, Therapeutic trends in pancreatic ductal adenocarcinoma (PDAC). *Expert Opin. Investig. Drugs* **28**, 161–177 (2019).
2. A. N. Hosein, R. A. Brekken, A. Maitra, Pancreatic cancer stroma: An update on therapeutic targeting strategies. *Nat. Rev. Gastroenterol. Hepatol.* **17**, 487–505 (2020).
3. H. Z. Wu, J. Q. Xiao, S. S. Xiao, Y. Cheng, KRAS: A promising therapeutic target for cancer treatment. *Curr. Top. Med. Chem.* **19**, 2081–2097 (2019).
4. A. M. Waters, C. J. Der, KRAS: The critical driver and therapeutic target for pancreatic cancer. *Cold Spring Harb. Perspect. Med.* **8**, a031435 (2018).
5. W. Shen *et al.*, TGF-β in pancreatic cancer initiation and progression: Two sides of the same coin. *Cell Biosci.* **7**, 39 (2017).
6. K. M. Mann, H. Ying, J. Juan, N. A. Jenkins, N. G. Copeland, KRAS-related proteins in pancreatic cancer. *Pharmacol. Ther.* **168**, 29–42 (2016).
7. H. C. Crawford, M. Pasca di Magliano, S. Banerjee, Signaling networks that control cellular plasticity in pancreatic tumorigenesis, progression, and metastasis. *Gastroenterology* **156**, 2073–2084 (2019).
8. B. R. da Cunha *et al.*, Cellular interactions in the tumor microenvironment: The role of secretome. *J. Cancer* **10**, 4574–4587 (2019).
9. H. Haslene-Hox, O. Tenstad, H. Wiig, Interstitial fluid-a reflection of the tumor cell microenvironment and secretome. *Biochim. Biophys. Acta* **1834**, 2336–2346 (2013).
10. P. Gromov *et al.*, Tumor interstitial fluid - a treasure trove of cancer biomarkers. *Biochim. Biophys. Acta* **1834**, 2259–2270 (2013).
11. C. Matas-Nadal *et al.*, Evaluation of tumor interstitial fluid-extraction methods for proteome analysis: Comparison of biopsy elution versus centrifugation. *J. Proteome Res.* **19**, 2598–2605 (2020).
12. J. A. Espinoza *et al.*, Cytokine profiling of tumor interstitial fluid of the breast and its relationship with lymphocyte infiltration and clinicopathological characteristics. *OncoImmunology* **5**, e1248015 (2016).
13. S. Onsurathum *et al.*, Proteomics detection of S100A6 in tumor tissue interstitial fluid and evaluation of its potential as a biomarker of cholangiocarcinoma. *Tumour Biol.* **40**, 1010428318767195 (2018).
14. L. Y. Lee *et al.*, Fascin is a circulating tumor marker for head and neck cancer as determined by a proteomic analysis of interstitial fluid from the tumor microenvironment. *Clin. Chem. Lab. Med.* **53**, 1631–1641 (2015).
15. C. C. DuFort, K. E. DelGiorno, S. R. Hingorani, Mounting pressure in the microenvironment: Fluids, solids, and cells in pancreatic ductal adenocarcinoma. *Gastroenterology* **150**, 1545–1557 e1542 (2016).
16. R. Kandimalla *et al.*, A 15-gene immune, stromal, and proliferation gene signature that significantly associates with poor survival in patients with pancreatic ductal adenocarcinoma. *Clin. Cancer Res.* **26**, 3641–3648 (2020).
17. A. Hauge, E. K. Rofstad, Antifibrotic therapy to normalize the tumor microenvironment. *J. Transl. Med.* **18**, 207 (2020).
18. M. R. Sullivan *et al.*, Quantification of microenvironmental metabolites in murine cancers reveals determinants of tumor nutrient availability. *eLife* **8**, 8 (2019).
19. J. Jung *et al.*, Generation and molecular characterization of pancreatic cancer patient-derived xenografts reveals their heterologous nature. *Oncotarget* **7**, 62533–62546 (2016).
20. J. Jung *et al.*, Novel cancer gene variants and gene fusions of triple-negative breast cancers (TNBCs) reveal their molecular diversity conserved in the patient-derived xenograft (PDX) model. *Cancer Lett.* **428**, 127–138 (2018).

21. H. Inohara, A. Raz, Identification of human melanoma cellular and secreted ligands for galectin-3. *Biochem. Biophys. Res. Commun.* **201**, 1366–1375 (1994).
22. P. S. Linsley *et al.*, Identification of a novel serum protein secreted by lung carcinoma cells. *Biochemistry* **25**, 2978–2986 (1986).
23. S. Iacobelli, E. Arnò, A. D'Orazio, G. Coletti, Detection of antigens recognized by a novel monoclonal antibody in tissue and serum from patients with breast cancer. *Cancer Res.* **46**, 3005–3010 (1986).
24. P. Stampolidis, A. Ullrich, S. Iacobelli, LGALS3BP, lectin galactoside-binding soluble 3 binding protein, promotes oncogenic cellular events impeded by antibody intervention. *Oncogene* **34**, 39–52 (2015).
25. X. Zhang *et al.*, Increased LGALS3BP promotes proliferation and migration of oral squamous cell carcinoma via PI3K/AKT pathway. *Cell. Signal.* **63**, 109359 (2019).
26. T. W. Lin *et al.*, Galectin-3 binding protein and galectin-1 interaction in breast cancer cell aggregation and metastasis. *J. Am. Chem. Soc.* **137**, 9685–9693 (2015).
27. K. Kim, Y. Kim, Preparing multiple-reaction monitoring for quantitative clinical proteomics. *Expert Rev. Proteomics* **6**, 225–229 (2009).
28. A. Salajegheh *et al.*, The expression profiles of the galectin gene family in primary and metastatic papillary thyroid carcinoma with particular emphasis on galectin-1 and galectin-3 expression. *Exp. Mol. Pathol.* **96**, 212–218 (2014).
29. V. Gopalan *et al.*, The expression profiles of the galectin gene family in colorectal adenocarcinomas. *Hum. Pathol.* **53**, 105–113 (2016).
30. T. Kobayashi *et al.*, Transient gene silencing of galectin-3 suppresses pancreatic cancer cell migration and invasion through degradation of β-catenin. *Int. J. Cancer* **129**, 2775–2786 (2011).
31. A. D. Rhim *et al.*, Stromal elements act to restrain, rather than support, pancreatic ductal adenocarcinoma. *Cancer Cell* **25**, 735–747 (2014).
32. K. L. Wu *et al.*, Extracellular galectin-3 facilitates colon cancer cell migration and is related to the epidermal growth factor receptor. *Am. J. Transl. Res.* **10**, 2402–2412 (2018).
33. H. Y. Kuo *et al.*, Galectin-3 modulates the EGFR signalling-mediated regulation of Sox2 expression via c-Myc in lung cancer. *Glycobiology* **26**, 155–165 (2016).
34. J. Merlin *et al.*, Galectin-3 regulates MUC1 and EGFR cellular distribution and EGFR downstream pathways in pancreatic cancer cells. *Oncogene* **30**, 2514–2525 (2011).
35. T. Troiani *et al.*, Targeting EGFR in pancreatic cancer treatment. *Curr. Drug Targets* **13**, 802–810 (2012).
36. S. Diersch *et al.*, Kras(G12D) induces EGFR-MYC cross signaling in murine primary pancreatic ductal epithelial cells. *Oncogene* **35**, 3880–3886 (2016).
37. N. M. Sodir *et al.*, MYC instructs and maintains pancreatic adenocarcinoma phenotype. *Cancer Discov.* **10**, 588–607 (2020).
38. J. C. Almagro, M. Pedraza-Escalona, H. I. Arrieta, S. M. Pérez-Tapia, Phage display libraries for antibody therapeutic discovery and development. *Antibodies (Basel)* **8**, E44 (2019).
39. H. Manceau, K. Amrani, K. Peoc'h, Personalized medicine, pharmacogenomic and companion biomarker. *Ann. Biol. Clin. (Paris)* **75**, 631–636 (2017).
40. T. J. George Jr., O. O. Ogunwobi, W. Sheng, Z. H. Fan, C. Liu, "Tissue is the issue": Circulating tumor cells in pancreatic cancer. *J. Gastrointest. Cancer* **45** (suppl. 1), 222–225 (2014).
41. J. Jung, H. S. Seol, S. Chang, The generation and application of patient-derived xenograft model for cancer research. *Cancer Res. Treat.* **50**, 1–10 (2018).
42. P. L. Garcia, A. L. Miller, K. J. Yoon, Patient-derived xenograft models of pancreatic cancer: Overview and comparison with other types of models. *Cancers (Basel)* **12**, E1327 (2020).
43. C. W. Hsu *et al.*, Proteomic profiling of paired interstitial fluids reveals dysregulated pathways and salivary NID1 as a biomarker of oral cavity squamous cell carcinoma. *Mol. Cell. Proteomics* **18**, 1939–1949 (2019).
44. A. Dokala, S. S. Thakur, Extracellular region of epidermal growth factor receptor: A potential target for anti-EGFR drug discovery. *Oncogene* **36**, 2337–2344 (2017).
45. D. Szklarczyk *et al.*, STRING v11: Protein-protein association networks with increased coverage, supporting functional discovery in genome-wide experimental datasets. *Nucleic Acids Res.* **47** (D1), D607–D613 (2019).
46. F. Giansanti *et al.*, Secreted Gal-3BP is a novel promising target for non-internalizing Antibody-Drug Conjugates. *J. Control. Release* **294**, 176–184 (2019).
47. T. Piyush *et al.*, Interaction of galectin-3 with MUC1 on cell surface promotes EGFR dimerization and activation in human epithelial cancer cells. *Cell Death Differ.* **24**, 1937–1947 (2017).
48. H. Blanchard, X. Yu, P. M. Collins, K. Bum-Erdene, Galectin-3 inhibitors: A patent review (2008-present). *Expert Opin. Ther. Pat.* **24**, 1053–1065 (2014).
49. Y. Yao *et al.*, HH1-1, a novel Galectin-3 inhibitor, exerts anti-pancreatic cancer activity by blocking Galectin-3/EGFR/AKT/FOXO3 signaling pathway. *Carbohydr. Polym.* **204**, 111–123 (2019).
50. T. Jeethy Ram, A. Lekshmi, T. Somanathan, K. Sujathan, Galectin-3: A factotum in carcinogenesis bestowing an archery for prevention. *Tumour Biol.* **43**, 77–96 (2021).
51. V. Loimaranta, J. Hepojoki, O. Laaksoaho, A. T. Pulliainen, Galectin-3-binding protein: A multitask glycoprotein with innate immunity functions in viral and bacterial infections. *J. Leukoc. Biol.* **104**, 777–786 (2018).
52. V. Lodermeyer *et al.*, The antiviral activity of the cellular glycoprotein LGALS3BP/90K is species specific. *J. Virol.* **92**, e00226-18 (2018).
53. O. Strobel, J. Neoptolemos, D. Jäger, M. W. Büchler, Optimizing the outcomes of pancreatic cancer surgery. *Nat. Rev. Clin. Oncol.* **16**, 11–26 (2019).
54. X. Xie *et al.*, Fe3O4-solamargine induces apoptosis and inhibits metastasis of pancreatic cancer cells. *Int. J. Oncol.* **54**, 905–915 (2019).
55. Y. Guan *et al.*, G-rich oligonucleotides inhibit HIF-1alpha and HIF-2alpha and block tumor growth. *Mol. Ther.* **18**, 188–197 (2010).
56. A. S. Leal *et al.*, Bromodomain inhibitors, JQ1 and I-BET 762, as potential therapies for pancreatic cancer. *Cancer Lett.* **394**, 76–87 (2017).
57. D. Gu *et al.*, Simultaneous inhibition of MEK and Hh signaling reduces pancreatic cancer metastasis. *Cancers (Basel)* **10**, E403 (2018).
58. M. Edderkaoui *et al.* An inhibitor of GSK3B and HDACs kills pancreatic cancer cells and slows pancreatic tumor growth and metastasis in mice. *Gastroenterology* **155**, 1985–1998 e1985 (2018).
59. N. S. Sharma *et al.*, Targeting tumor-intrinsic hexosamine biosynthesis sensitizes pancreatic cancer to anti-PD1 therapy. *J. Clin. Invest.* **130**, 451–465 (2020).
60. B. A. Johnson III, M. Yarchoan, V. Lee, D. A. Laheru, E. M. Jaffee, Strategies for increasing pancreatic tumor immunogenicity. *Clin. Cancer Res.* **23**, 1656–1669 (2017).
61. H. S. Ahn *et al.*, Convergence of plasma metabolomics and proteomics analysis to discover signatures of high-grade serous ovarian cancer. *Cancers (Basel)* **12**, E3447 (2020).
62. J. Andris-Widhopf, C. Rader, P. Steinberger, R. Fuller, C. F. Barbas III, Methods for the generation of chicken monoclonal antibody fragments by phage display. *J. Immunol. Methods* **242**, 159–181 (2000).
63. Y. Lee, H. Kim, J. Chung, An antibody reactive to the Gly63-Lys68 epitope of NT-proBNP exhibits O-glycosylation-independent binding. *Exp. Mol. Med.* **46**, e114 (2014).